Hemin binding causes structural rearrangements in HRI to inhibit activation via autophosphorylation

Authors: Shivani Kanta[1], Vanesa Vinciauskaite[1], Graham Neill[1], Miratul M.K. Muqit[2], Glenn R. Masson[1*]

1 = Division of Cellular and Systems Medicine, School of Medicine, University of Dundee, Dundee, DD1 9SY, United Kingdom.
2= MRC Protein Phosphorylation and Ubiquitylation Unit, School of Life Sciences, University of Dundee, Dundee, DD1 5EH, UK

*= corresponding author email: gmasson001@dundee.ac.uk

Abstract

Heme-Regulated Inhibitor (HRI) is one of the four mammalian kinases which phosphorylates eIF2α to facilitate a cellular response to stress through the regulation of mRNA translation. Originally identified for its role as a heme sensor in erythroid progenitor cells, it has since materialised as a potential therapeutic target in both cancer and neurodegeneration. Here we characterise two modes of HRI inhibition of using structural mass spectrometry, biochemical and biophysical techniques. We demonstrate that several ATP-mimetic compounds, including BRAF inhibitors and a compound, GCN2iB, thought to be specific to GCN2, are capable of potently inhibiting HRI. We demonstrate that hemin, a haem-like molecule, inactivates HRI structurally using hydrogen-deuterium exchange mass spectrometry (HDX-MS), and this results in wide-spread structural rearrangement of the protein and how that impacts on the kinase domain through a series of allosteric interactions. This inhibition mainly impacts autophosphorylation, which includes tyrosine phosphorylation, not observed before in the eIF2α kinases.

Introduction

Heme-Regulated Inhibitor (HRI) was first identified as a key regulator in erythroid cells, where it activates the Integrated Stress Response (ISR) in response to heme deprivation during terminal erythropoiesis[1,2], facilitating the balanced translation of the alpha-globin and beta-globin chains in response to fluctuating iron levels[2]. The current model of how HRI is activated is thought to be through an inhibitory interaction with heme, which dissociates upon cellular heme depletion, allowing HRI to become active[3–5]. Once activated, HRI phosphorylates its substrate – the alpha subunit of the eukaryotic initiation factor eIF2- eIF2α on Serine 51 (in higher eukaryotes), resulting in the activation of the ISR and the upregulation of the transcription factor ATF4.

More recently, HRI activity has been shown to be a regulator of mitochondrial stress and mitophagy, the autophagic elimination of mitochondria[6–10]. This is thought to occur primarily through the signalling factor DELE1 (DAP-3 binding cell death enhancer 1). Upon mitochondrial stress, the inner mitochondrial membrane protease OMA1 is activated, which in turn promotes the cleavage of DELE1. The resulting C-terminal fragment may then oligomerise and accumulate in the cytosol, which then results in the activation of HRI and activation of the ISR. Furthermore, HRI activity may impact on PINK1 kinase activity, mutation of which is causative for Parkinson's Disease[11,12]. Currently it is unknown how DELE1 stimulates HRI, and whether this is dependent upon heme release. In additional to mitophagy, it has been shown that HRI also has a role in wider proteostasis. HRI may be activated upon proteasomal inhibition (via compounds such as bortezomib) to facilitate proteasomal-independent protein degradation via the lysosome and the eventual development of resistance[13–15]. Although the exact mechanism of how HRI may be activated within this context is yet to be elucidated.

Altering HRI activity may be beneficial in the context of cancer[14,16–19], as over-activation of the ISR may lead to highly selective CHOP mediated apoptosis in cancer cells. This has led to the development of compounds capable of activating HRI – namely the 1-((1,4-trans)-4-aryloxycyclohexyl)-3-arylureas (cHAUs) and the N,N'-diarylureas (such as 1-(benzo[d][1,2,3]thiadiazol-6-yl)-3-(3,4-dichlorophenyl)urea, or BTdCPU)- however, their exact mechanism of how they activate HRI has remained elusive, with most studies being conducted within a cellular context [16,20–23]. Conversely, there may also be therapeutic potential in inhibiting the ISR and HRI in cancer, as constitutive activation of the pathway may promote cancer cell survival [14,16,17,24,25].

Given HRI's role in translation, cancer and neurodegeneration, we have investigated the mechanisms of autophosphorylation, activation and inhibition of human HRI. We were able to demonstrate that HRI is inhibited by the clinically approved RAF inhibitors (RAFi) small molecules Dabrafenib and Encorafenib, but not LY3009120. Additionally, we were also able to demonstrate that GCN2iB, a tool compound used to selectively inhibit the related eIF2α kinase GCN2[26], is a highly potent inhibitor of HRI. We were unable to demonstrate any direct *in vitro* effect of the small molecule activator BTdCPU – a well characterised activator of HRI in cells, suggesting this compound activates HRI indirectly as had been recently reported[10]. Using Hydrogen Deuterium Exchange Mass Spectrometry (HDX-MS), we characterised the mechanisms of both the inhibitory heme analogue Hemin, and the BRAF inhibitor Dabrafenib, and showed that although they exhibit distinct mechanisms of action, they both ultimately impact on shared aspects of the kinase domain. We show that this inhibition results in a loss of autophosphorylation, including tyrosine residues, which was unexpected. Our data support that heme binding results in a large-scale rearrangement of the protein, with likely additional folding events of disordered segments, and may provide insight into how inhibitors of HRI may be developed in the future.

Results

HRI Oligomerization State is Phosphorylation Independent

N-terminally His-Tagged human HRI was purified from *Escherichia coli (E. coli)* cells using affinity chromatography, followed by ion exchange chromatography, and subsequent gel filtration (See Figure 1A) (*4*). Gel filtration (Figure 1B) suggested the protein was homodimeric. SDS-PAGE analysis of the material purified from *E.coli* demonstrated that HRI (monomeric molecular weight: 75017 Da) migrated to >85kDa, suggesting post-translational modification. Treatment with lambda protein phosphatase caused the HRI band to shift back to ~75 kDa on the SDS-PAGE – this observation being reported previously (*4*, *19*) (Figure 1A).

We next conducted mass photometry analysis on HRI in both dephosphorylated and autophosphorylated forms to determine whether phosphorylation facilitated any changes in the oligomeric state (Figure 1C). We observed two peaks, a predominant peak with an average mass of approximately 150 kDa, indicative of a dimer, and a second minor peak of a possible quaternary state (with a mass of ~350 kDa). There was little difference in the relative abundances of these peaks for both dephosphorylated and phosphorylated HRI, suggesting autophosphorylation does not drive dimerization/oligomerisation as previously reported[3].

HRI undergoes extensive autophosphorylation

We determined that HRI was extremely active using kinase assays against recombinantly purified human eIF2α (Figures 1D & E). Using Phos-tag gels we were able to track both autophosphorylation and substrate phosphorylation (Figure 1E) – even with nanomolar concentrations of HRI, at very short time points, with the reactions conducted on ice, we found that HRI autophosphorylated rapidly such that the reaction rates against eIF2α between phosphorylated and dephosphorylated HRI were largely indistinguishable (i.e. there was no “lag” autophosphorylation phase). Nonetheless, using the Phos-tag gels, we were able to visualise the gradual autophosphorylation of HRI over 10 minutes.

To investigate the locations HRI autophosphorylation sites, we first dephosphorylated HRI using lambda phopsphatase, removed the phosphatase by gel filtration, and then incubated this dephosphorylated HRI with ATP induce autophosphorylation. Autophosphorylated HRI was then analysed by mass spectrometry to determine sites of phosphorylation. In total 41 sites of autophosphorylation were detected (Figure 1F, Supplementary Data 1, Table 1) – these are sites which could be determined unambiguously in all three repeats and had high stringency criteria. Unexpectedly, we detected numerous phosphotyrosine residues. Crucially we detected the phosphorylation of T486 and T488 – two residues found within the activation loop and previously identified in mice (Mouse residues T483 and T485) as critical for autophosphorylation activity[27].

To interpret the locations of these phosphorylated residues on HRI, we used AlphaFold 3 to create a prediction of the structure of dimeric HRI [28] (Figure 1G/H). This prediction placed the kinase domains in a back-to-back conformation, with Heme Binding Domains (HBD) in similar positions “on top” of the kinase domain, with the coiled coil domain situated beneath.

HRI can be inhibited by RAFi compounds and GCN2iB

Previous studies have used the heme analogue hemin to investigate how iron levels may impact HRI activity[3]. We were able to track both HRI autophosphorylation and eIF2α phosphorylation in the presence of hemin and produced an IC_{50} value of 2.87 μM ± 1.28, which agrees with previous studies[3,29] (Figure 2A/B/C). We were unable to achieve “complete” inhibition of HRI (as measured by ADP production) using hemin, an observation previously described [3], with a residual ~25% ATPase activity detected even at very high hemin concentrations (>200 μM). Western-blot analysis of HRI found that hemin functionally blocked autophosphorylation, but there was still residual phosphorylation of eIF2α (Figure

2B). We then used differential scanning fluorimetry (DSF) to determine the effects of compound binding on HRI stability (Figure 2F). We were able to detect an HRI unfolding event with a T_m of 51.0 ± 0.1 ºC and the addition of 5 µM Hemin caused no significant difference to protein stability (50.7 ± 0.3 ºC), as has also been previously reported[3].

It has been reported that small molecule inhibitors of BRAFV600E (RAFi compounds) may have activity against the amino acid stress sensing eIF2α kinase General Control Nonderepessible 2 (GCN2) [30,31]. Given the sequence homology between the kinase domains of HRI and GCN2 (See Supplementary Figure 1), we screened Dabrafenib, Encorafenib, and LY3009120, and the small molecule activator/inhibitor of GCN2, GCN2iB [26,32] to see whether they had any effect on HRI activity (Figure 2D and E). We found that two of the RAFi compounds, Dabrafenib and Encorafenib, were potent inhibitors of HRI, with sub-micromolar IC_{50} values, while LY3009120 had no effect on HRI activity. GCN2iB, was an extremely potent inhibitor of HRI with a sub-nanomolar affinity. Thermal stability analysisusing DSF (Figure 2F) showed significantly increased thermal stability to HRI on addition of 10 µM these compounds – Encorafenib increased the T_m by +4.35 ± 0.2 ºC, Dabrafenib +6.1 ± 0.8 ºC and GCN2iB +9.1 ± 0.4 ºC (Figure 2F).

Furthermore, we also screened the small molecule activator of GCN2 BTdCPU – a well-characterised activator of HRI [17,20–23,33]. Despite a wide range of concentrations and approaches being employed, we were unable to detect any of HRI changes in activity upon BTdCPU incubation (Figure 2C, Supplementary Figure 2). We found that BTdCPU could not overcome Hemin-induced inhibition, and that in the absence of Hemin, could not activate HRI. Addition of 10 µM BTdCPU caused no significant difference on HRI thermostability using nanoDSF analysis (50.8 ± 0.5 ºC) (Figure 2F).

Hemin and Dabrafenib binding result in distinct modes of HRI Inhibition

To gain insight into the mode of action of these inhibitors, we conducted Hydrogen Deuterium Exchange Mass Spectrometry (HDX-MS) in the absence or presence of 100 µM Dabrafenib/Hemin. We produced a peptide map of dephosphorylated human HRI consisting of 218 peptides, with a coverage of 89.3%, and average redundancy of 14.1. HDX-MS of Apo HRI identified that there were several unstructured loops maintained in dimeric HRI between residues 1-70, 143-153, 230-370, 467-495 and 583-593 (Figure 3A) – which corresponded well with the AlphaFold predicted structure (See Table 2.0).

Dabrafenib binding (see Figure 3B-E) caused a reduction in solvent exchange in four areas – a kinase inhibitor pocket consisting of residues 157-192, 209-229, 432-469 (Figure 3B, C, D,E) and intriguingly, the C-terminus residues 594-613 (Figure 3B). Single peptides covering the DFG loop – for example, residues 459-464, showed strong reduction in HDX, however neighbouring peptides (*e.g.* 448-456 and 467-475) showed no reduction suggesting a possible direct interaction between Dabrafenib and the DFG loop. Modelling of Dabrafenib in the HRI kinase domain was done using crystal structure PDB:5CSW [34], and this aligned well with HDX-MS data. Dabrafenib binding also produced an area of increased solvent exchange in Kinase 2 domain between residues 531-559.

Hemin binding resulted in very widespread alterations in the solvent exchange rate of HRI (Figure 4), suggesting a large structural rearrangement of the protein. Despite the concentration of Hemin being at saturating concentrations (100 µM), many HRI peptides exhibited bimodal distributions upon Hemin binding making data analysis and interpretation challenging (Figure 4B,C, D,E). The N-terminus of HRI which exhibited EX1 kinetics between residues 1-70 on hemin binding (Figure 4B/E)– previously the N-terminus of HRI has previously identified as to undergoing a structural reorganisation upon heme binding [3,35]. EX1 kinetics were also observed in the disordered region of 144-153, suggesting the possibility of a partial folding event occurring on hemin binding. Furthermore, within the kinase domain, 171-208 also exhibited EX1 kinetics, as well as the very C-terminus of HRI

(residues 596-613) addition of hemin – suggesting a widespread conformational change upon hemin binding. The large, disordered region of HRI – between residues 230 and 350, also demonstrated EX1 kinetics, with sub-populations of highly protected peptides emerging on HRI binding.

Several HRI peptides that exhibited “classical” EX2 exchange kinetics on Hemin binding with prototypical isotopic distributions also exhibited decreases– suggesting that incomplete hemin binding was not the root cause of the bimodal peptide populations. Within the kinase domain for example, there is a large reduction in solvent exchange around the activation loop (the “DFG” residues of 461-463) upon hemin binding (Figure 4D), and residues 113-127, which contain the Heme binding histidine residues H119 and H120, exhibited EX2 reductions in solvent exchange upon hemin binding (Figure 4E).

Discussion

Here we present insight into the activation and inhibition of HRI via biochemical analysis and structural mass spectrometry, providing insights into how heme-like compounds, ATP-mimetic inhibitors, and phosphorylation may work together to regulate this kinase.

The kinase domain of HRI has an unusual architecture, with a very prominent disordered insertion (residues 241-370) between the two lobes of the kinase domain, and a rather extended activating loop (residues 464 to 488), and the P-loop (residues 170-181) lacks a consensus Walker Motif A (typically G-x(4)-GK-[TS])[36] – HRI has a sequence of $_{166}$EFEELAIL<u>GK</u>GGY$_{178}$ with only the GK resides adhering to the consensus sequence. Opposite the P-loop, the activation loop harbours multiple sites of phosphorylation, including T486 and T488, which have been shown to be crucial for activation of the kinase[27]. Prior to this study, it was unclear how the heme-binding domains of HRI could facilitate the inhibition of HRI. We show in this study that there is likely a large intramolecular rearrangement of HRI caused by Heme binding, that ultimately prevents the kinase domain preventing autophosphorylation.

HRI is an extremely active kinase when released from Heme –experiments had to be conducted rapidly with low nanomolar concentrations of HRI on ice to observe the accumulation of substrate. Furthermore, HRI not only readily phosphorylates eIF2α, but also autophosphorylates rapidly. As many as 33 sites have been reported previously – although these studies were conducted in mice HRI [37], here in human HRI we report a total of 41 phosphorylation sites. Although mouse and human HRI have ~83% sequence homology (see Supplementary Figure 3), some of these sites of phosphorylation are unique to either species. There are two notable patches of dense phosphorylation – a section in the disordered insert (residues 275-309), and within the kinase activation loop of HRI. While phosphorylation of the activation loop is a common means of controlling kinase activation, in HRI we observed the phosphorylation of T486, T488, S489, T493, Y496 and S498, six residues within the 12 amino acids, representing a very dense patch of phosphorylation. Also of note is residue S615 on the coiled coil – this is very distal from the kinase domain and suggests either that this domain is attached to the rest of the enzyme on very flexible loops, or that the placement of the coiled coil is closer to the kinase domain.

Interestingly, we detected numerous phosphotyrosine modifications in the dataset; some have been detected before elsewhere[37], but the material analysed was purified in a manner which could not exclude the possibility of extraneous kinases modifying HRI. Of particular importance is the residue Y193 (mouse numbering) which was previously found to be critical for the activity of HRI [37] – a Y193F mutant had ~50% reduced activity of wtHRI. Here we identified the phosphorylation of both Y192 and Y193 (although in mice, Y192 is H192, preventing its phosphorylation). Our material, purified from *E. coli,* and subsequently dephosphorylated with lambda phosphatase leaves limited opportunity for these sites to be the result of extraneous phosphorylation. In future work it will be important to assess the stoichiometry of Tyr versus Ser/Thr autophosphorylation using mutagenesis and Phos-Tag analysis.

An example of a protein kinase family that can both tyrosine autophosphorylate and phosphorylate substrates on serine/threonine residues is the DYRK (dual specificity tyrosine-phosphorylation regulated kinase) family. These proteins have been shown to tyrosine autophosphorylate co-translationally and after translation as a mature protein[38]. It would be interesting to perform phosphomapping analysis of HRI in the absence of ATP incubation *in vitro* to determine whether HRI becomes tyrosine autophosphorylated whilst it is inside the *E. coli* cell and further experiments would need to be done to determine whether this can also be a co-translational event.

A key determinant of specificity for serine/threonine versus tyrosine kinases is a single amino acid in a region of the activation segment known as the P+1 loop[39]. In serine/threonine kinases, this residue is a serine or a threonine, and in tyrosine kinases, it is a proline essential for interacting with the phospho-acceptor tyrosine residue. In dual-specificity kinases, for example in the DYRKs, it is a serine[40], and in HRI T488 is followed by a serine ([481]GKRTPTHTSRV[491]), and several other features of the kinase domain point towards it being a Ser/Thr Kinase (e.g. the APE-6 "GT", the HRD+2 "K", and the lack of a doule YY at the DFG+10 position[41]). Other elements point towards Tyr/Kinase, e.g. HRD +4 "RN" [41]. Notably, the highly conserved "APE" element is found as ApSPE in HRI. Comparing HRI to the DYRK 1A/2/3, many sequences and residues are conserved namely the catalytic loop e.g. a "HRDLKPxNIxL" motif of the catalytic loop and a cysteine at the +2 position of the DFG (DFGxxC) – this cysteine is not present in the other eIF2α kinases (see Supplementary Figure 1). Mutagenesis and further structural studies may help elucidate how the HRI kinase domain is capable of tyrosine phosphorylation.

The discovery that the small molecule BRAF inhibitors Dabrafenib and Encorafenib are capable of inhibiting HRI *in vitro* is of interest. Given that both BRAF and HRI function as back-to-back kinase domains, it may be of interest to determine whether these compounds also exhibit the same concentration-dependent paradoxical activation behaviour as observed in BRAF [42]. We did not observe activation of HRI by these compounds, but given the extremely high activity of HRI, it may be difficult to detect any additional increase in activity. HDX-MS provides a clear indication of the binding site for Dabrafenib within the kinase domain (Figure 3-B/E), with multiple protections in the kinase site as would expected for a kinase inhibitor. There are reductions in solvent exchange in residues corresponding to both the P-loop (residues 170-183), the catalytic loop (441-449) and DFG motif 461-463) and part of the activating loop (464-508). The two crucial autophosphorylation residues of T486 and T488 showed no reduction in solvent exchange upon Dabrafenib binding – which may mean that these residues may be still capable of being phosphorylated, and potentially "activating" the enzyme while Dabrafenib is still bound.

Additionally, Dabrafenib caused an increase in solvent exchange rate in the kinase domain in residues 531-559. The role of these residues isn't readily apparent – they may contain a cryptic Walker B motif, although there is considerable variability in this motif. The region does contain resides T538, T542, and S548 all of which are autophosphorylated by HRI. Dabrafenib binding also resulted in the protection in part of the coiled-coil domain in residues 594-613. Given the predicted distance between the kinase domain and this section of the coiled coil, it is difficult to interpret this – other than the possibility that the placement of the coiled coil in the AlphaFold 3 model may be incorrect. This would also explain some aspects of heme binding data (see below)

Hemin binding appears to be an incomplete inhibitor of HRI. This has been reported previously [3–5], and here we show that hemin binding appears to be capable of preventing autophosphorylation while still allowing for some eIF2α phosphorylation (Figure 2B/C). This may be due to the fact that hemin is not heme – in a cellular context there will be variety of hemes which have different chemistries with different functional groups, and hemin contains ferric (Fe^{3+}) rather than ferrous (Fe^{2+}), as found in heme. It may well be that certain hemes are more potent inhibitors of HRI. However, we did find that hemin binding resulted in reductions in solvent exchange at H119/H120 – the proposed haem biding site of HRI [35]. A further conserved residue C411 (see supplementary figure 3) has been implicated in heme binding also. Although this exact residue did not appear to have a reduction in solvent exchange, the neighbouring helices of 416-426 and 392-408 both had reductions in solvent exchange (Figure 4D). Given the wide-spread EX1 kinetics resulting from large-scale domain reorganisation makes identifying the exact site of heme binding less robust. Overall, previous mutagenesis studies had also suggested that heme binding causes large-scale structural rearrangements of HRI[27,35,37,43], and this had been accompanied by changes in

helicity as measured by circular dichromatism[29]. Our data support this observation – the structure of HRI with heme bound may well be vastly different to that of unbound, autophosphorylated HRI.

Finally, BTdCPU has been widely used as an HRI activating compound [10,17,33] – although its mode of action was unclear – previous studies had suggested that N,N′-diarylureas were capable of directly binding and activating HRI[23]. Throughout our studies on HRI, we were unable to detect direct binding or activation with BTdCPU under numerous differing conditions (Supplementary Figure 2). To facilitate HRI activation, the previously suggested model would require BTdCPU to displace a heme molecule to facilitate activation – this would require a K_d of < 1 μM, but we were unable to detect any binding or effect on HRI activity even at concentrations greater than 100 μM. This agrees with a recently published study by Perea *et al.* who demonstrated that HRI activation via BTdCPU functioned via mitochondrial decoupling and subsequent OMA1-DELE1 signalling, rather than direct interaction with HRI [10].

Given the expanding role of HRI in mitochondrial stress sensing[6–10,12], it is likely that there will be renewed interest in targeting HRI in disease. Our data here show potential for BRAF-like compounds as inhibitors as a starting point for pharmaceutical development – however there is the distinct possibility that these compounds may also activate HRI via paradoxical inhibitor activation mechanisms [26,44]. Further structural work is necessary to understand HRI, as current predicted models fail to completely explain the structural changes observed with both heme and inhibitor binding. This study also raises the possibility that HRI may catalyse tyrosine phosphorylation also – mutagenesis and phosphoproteomics work will be necessary to see whether this is maintained *in vivo*.

Figure Legends

Figure 1: Characterisation of the phosphorylated HRI dimer (A): Purified recombinant HRI run on an SDS-PAGE gel in both phosphorylated (P) and lambda protein phosphate dephosphorylated (NP) form *(B)* Size-Exclusion Chromatography (Superdex 200i 10/300 GL) of phosphorylated and dephosphorylated HRI both of which elute with a retention volume of 10.47 mL *(C)* Mass Photometry analysis of HRI. Both P and NP HRI have a predominant population of ~150 kDa, indicative of a dimeric state. *(D)* ADP-GLO Kinase assay of HRI P and NP. *(E)* Phos-Tag Gel of HRI assay. Both phosphorylation of substrate (recombinant human eIF2α) and autophosphorylation are observed. (*F)* Sites of HRI autophosphorylation. (*G)* AlphaFold 3 model of Apo HRI dimer, with domains highlighted. The dashed line shows the approximate line of 2-fold symmetry. (*H)* Locations of autophosphorylated residues on HRI, with those on the periphery of highlighted.

Figure 2: Characterisation of HRI modulators (A) ADP-GLO kinase assay with a concentration gradient of hemin using recombinant eIF2α as a substrate– an IC_{50} of 2.87 ± 1.28 μM was determine. No activity was detected in the absence of HRI (eIF2α only control). *(B)* Western-Blot assay acquired from a Phos-Tag separated HRI kinase assay using eIF2α substrate to observe Hemin effects on both autophosphorylation and substate phosphorylation. The total eIF2α probe shows the development of phosphorylated eIF2α over the course of the reaction, reduced in the presence of Hemin. The S51 phosphorylation specific antibody probe shows the gradual production of phosphorylated substrate from HRI. HRI moves to a higher band (indicative of phosphorylation) upon addition of ATP – this is inhibited upon addition of Hemin. *(C)* Phos-tag analysis of the effects of Hemin and BTdCPU on eIF2α phosphorylation. *(D)* Phos-tag analysis of RAFi and GCN2iB. *(E)* ADP-GLO analysis of HRI activity against RAFi and GCN2iB. *(F)* nanoDSF analysis of 5 μM Hemin, 10 μM BTdCPU, 10 μM Dabrafenib, 10 μM Encorafenib and 10 μM GCN2iB. T_Ms (as determined as the nadir of the first derivative of the ratio of the 350/ 330 nm curve) are shown above.

Figure 3: HDX-MS analysis of Dabrafenib Binding (A) Global Exchange profile of Apo Dimeric dephosphorylated HRI over five timepoints. The dashed line at 50% - typically peptides with >50% exchange at the 0.3s timepoint (blue points) are disordered regions *(B)* HRI kinase domain with Dabrafenib binding modelled. Peptides which exhibited a reduction of solvent exchange upon Dabrafenib binding are highlighted in blue. (*C*) Inset of the kinase domain of HRI, showing solvent exchange changes upon Dabrafenib binding. Dabrafenib docked using a BRAF model (PDB:5CSW) *(D)* HDX-MS plot of Dabrafenib binding to HRI. Summed difference over all five timepoints *(E)* Selected peptides exhibiting differences in solvent uptake upon Dabrafenib binding. * = > 5%/0.5Da difference and passes a student t-test with p </= 0.05.

Figure 4: HDX-MS analysis of Hemin Binding (A) A selection of peptides detailing the solvent uptake differences upon Hemin and Dabrafenib binding. * = > 5%/0.5Da difference and passes a student t-test with p = 0.05 (or lower) with Dabrafenib binding when compared to Apo HRI. # = > 5%/0.5Da difference and passes a student t-test with p = 0.05 (or lower) with Hemin binding when compared to Apo HRI. *(B)* Spectra of selected peptides exhibiting EX1 kinetics which emerge on Hemin binding. (*C*) HDX-MS data mapped onto an AlphaFold Model with Heme docking. Representations of EX1 kinetics in three peptides found within the regions indicated as pink. (*D*) Kinase domain upon Hemin binding. (*E*) HDX-MS data around the Heme Binding Domain. Two previously identified residues, Histidine 119 and 120, are highlighted and represented as spheres.

Supplementary Figure 1: Alignment of the kinase domains of all the human eIF2α kinases (PKR, PERK, HRI and GCN2).

397 *Supplementary Figure 2:* BTdCPU kinase assays. (A) Activity of HRI (as measured by ADP
398 production) on the addition of increasing BTdCPU in either the absence or presence of
399 Hemin. (B) Autophosphorylated HRI (i.e. HRI pre-incubated with ATP and subsequently
400 purified) was exposed to increasing BTdCPU in the presence of eIF2α. ADP levels were
401 measured using ADP-GLO and plotted as a % of APO HRI-P levels.
402
403 *Supplementary Figure 3:* Species alignment of HRI. Human (*H. sapiens*), Mouse (*M.*
404 *musculus)*, Rat (*R. ratus)*, Rabbit (RABIT) and *Macaca fascicularis* (Crab-eating macaque)
405 (Cynomolgus monkey) of EIF2AK1 (HRI).
406
407

408
409 **Materials and Methods**
410
411 *HRI Expression and Purification* Briefly Human HRI cDNA was obtained from the MRC
412 Protein Phosphorylation and Ubiquitination Unit (MRC PPU) was subcloned into a pOPTH
413 plasmid with an N-terminal 6His TEV-cleavable tag. Protein was expressed in BL21-
414 Rosetta(DE3) (Novagen) *E. coli*. Cells were grown at 37 ºC in 2xTY media until an
415 absorbance of 0.7 at 600 nm was achieved, where protein expression was induced on the
416 addition of 0.8 mM IPTG. Cells were left to express protein for 16 h at 18 ºC. A pellet
417 generated from 3 L of media was lysed in 100 mL Lysis Buffer (20 mM Tris pH 8.0, 500 mM
418 NaCl, 20 mM Imidazole, 2 mM beta-mercaptoethanol (BME), with 1 µL benzonase,
419 (Novagen) and 2 EDTA-free Protease inhibitor tablet (PROMEGA)) via probe sonication (10s
420 ON/ 10s OFF at 60% amplitude, on ice). Lysate was centrifuged at 4 ºC at 40,000 *g* for 45
421 minutes. The supernatant was filtered through a 0.45 nm filter and then loaded onto a 5 mL
422 HisTrap HP Column (Cytiva) equilibrated in Lysis Buffer. After washing with 10 column
423 volumes with lysis buffer and a mAU of <100 of achieved, a gradient of NiNTA Buffer B
424 Buffer (20 mM Tris pH 8.0, 500 mM NaCl, 200 mM Imidazole pH 8.0, 2 mM BME) was
425 applied. Fractions were analysed using SDS-PAGE to determine HRI-containing fractions.
426 HRI containing fractions were then diluted 1:1 with Q_O Buffer (20 mM Tris pH 8.0, 2 mM
427 BME), and then passed over a 5 mL Q HP (Cytiva) column, equilibrated in Q_A Buffer (20 mM
428 Tris pH 8.0, 100 mM NaCl, 2 mM BME), at a rate of 2 ml/min. A gradient of increasing Q_B
429 buffer (20 mM Tris pH 8.0, 1 M NaCl, 2 mM BME) was then initiated, with HRI eluting at
430 approximately 600 mM NaCl. HRI containing fractions were then concentrated using a
431 VIVASPIN 10k MWCO Concentrator (Sartorius) until a volume of <1 mL was produced. We
432 then dephosphorylated HRI using Lambda Protein Phosphatase (Lambda PP (New England
433 Biolabs)), with 800 units of phosphatase, and the reaction left at 4 ºC for 16 hours. Finally,
434 dephosphorylated HRI was injected onto a Superdex 200i GL 10/30 (Cytiva) equilibrated in
435 Gel Filtration Buffer (20 mM HEPES pH 7.5, 150 mM NaCl, 2 mM TCEP). HRI containing
436 fractions, eluting at ~10.5 mL, were pooled and concentrated with a VIVASPIN 10k MWCO
437 Concentrator (Sartorius) until a concentration of 1.5 mg/mL was achieved. HRI was then
438 frozen in liquid nitrogen at stored at -70 ºC.
439
440 *eIF2α Expression and Purification* Expression and purification of recombinant human eIF2α
441 was conducted as described previously[45]. DNA encoding full-length human eIF2α (NCBI
442 reference number: NP_004085.1) was inserted into the vector pOPTH with an N-terminal
443 His6 tag followed by a TEV protease site. The plasmid was transformed into chemically
444 competent BL21 Star (DE3) cells, and cells were grown overnight before being inoculated to
445 a 50 mL starter culture in 2xTY media containing 0.1 mg/mL Ampicillin. The starter culture
446 was incubated at 37 ˚C for 90 minutes, then 10 mL starter culture was added to 4 x 900 mL
447 2xTY media containing Ampicillin. Cultures were incubated at 37 ˚C until the optical density
448 reached 0.7, and then protein expression was induced by the addition of 0.3 mM isopropyl β-
449 D-1- thiogalactopyranoside (IPTG). Cells were grown for a further 3 hours at 37 ˚C before
450 being harvested, washed with ice-cold phosphate-buffered saline and frozen in liquid
451 nitrogen.
452
453 Bacterial cell pellets were lysed in 100 mL Lysis Buffer (20 mM Tris-HCl pH 8.0, 100 mM
454 NaCl, 5 % v/v glycerol, 2 mM BME 0.5 mg/mL Lysozyme (Sigma L6876), 2 U/mL Benzonase
455 , one cOmplete EDTA-free protease inhibitor tablet (Roche 04693132001) per 50 mL of
456 Buffer). Cells were lysed using a probe sonicator for 5 minutes (10 s on/ 10 s off) and then
457 centrifuged at 140,000 *g* for 45 min at 4 ˚C. The supernatant was filtered through a 0.2 µm
458 syringe filter before being loaded onto a 5 mL HisTrap HP Column (Cytiva 17524801)
459 equilibrated in Ni A Buffer (20 mM Tris pH 8.0, 100 mM NaCl, 5 % v/v glycerol, 10 mM
460 imidazole pH 8.0, 2 mM BME), followed by the elution of protein via a gradient of Ni B Buffer
461 (20 mM Tris pH 8.0, 100 mM NaCl, 5% v/v glycerol, 200 mM Imidazole pH 8.0, 2 mM BME).

462 Protein purification then proceeded as described for HRI. Proteins were concentrated to ~10
463 mg/mL and then snap frozen in liquid nitrogen.
464
465 *Phos-tag Assays:* 250 nM HRI incubated with 8 μM eIF2α and 100 μM ATP in Kinase
466 Reaction Buffer (20 mM HEPES pH 7.5, 150 mM NaCl, 5 mM $MgCl_2$, 1 mM TCEP) for stated
467 time at either room temperature or on ice. Hemin (Selleckchem S5645) was dissolved in 10
468 mM NaOH(*4*). Reactions were terminated through the addition of an equal volume of 2 x
469 Phos-tag Loading Buffer (0.1 M Tris pH 6,5, 0.2 M DTT, 4% w/v SDS, 15% Glycerol, 1 mM
470 $ZnCl_2$). Precast 17-well Phos-tag gels (SuperSep PhosTag (50 μmol/L) FujiFilm 192-
471 18001/199-18011) were loaded with 10 μL of the reaction/Loading buffer solution in the
472 suggested running buffer (0.1 M Tris Base, 0.1 M MOPS, 0.1% SDS-PAGE, 1 mM $NaHSO_3$).
473 Gels were run for 1 hour at 150 V and stained using Quick Coomassie Stain (Generon).
474
475 *Western Blots:* For Phos-tag Assays, gels were wash three times in transfer buffer (25 mM
476 Tris, 190 mM Glycine, 10% Methanol, pH 8.3) with 10 mM EDTA. Proteins were transferred
477 using wet transfer. All blocking buffers were 4% BSA in TBST. Antibodies used: HRI
478 (Invitrogen 7H3L3, Rabbit, 1:500), Total eIF2α (Santa Cruz Biotechnology, SC-133132,
479 1:500), pSer51 eIF2α (Cell Signalling Technology 9721S, 1:250), IRDye680 Goat anti
480 Mouse (Licor 926-68070), IRDye 800CW Donkey Anti Rabbit (Licor 926-32213). All images
481 taken using Licor Odyssey FC system and images analysed using ImageStudio. Blots
482 representative of a minimum of three repeats.
483
484 *ADP-GLO Kinase Assays:* Using a PROMEGA ADP-GLO Kinase assay, HRI was incubated
485 with eIF2α and ATP at the stated concentrations in Kinase Reaction Buffer (20 mM HEPES
486 pH 7.5, 150 mM NaCl, 5 mM $MgCl_2$, 1 mM TCEP) for the stated time at room temperature,
487 until the reaction was quenched using the ADP-GLO Reagent. 4 μL kinase reactions were
488 conducted in Corning 3824 wells before quenching and development using the ADP-
489 GLO/Kinase Detection Reagent as per the manufacturer's instructions. An ADP/ATP curve
490 was created using the kit for calculation of relative ADP concentrations after kinase reaction
491 quenches. Luminescence measured using a Pherastar CLARIOstar (BMG LABTECH). Data
492 analysis conducted using Graphpad Prism 10 (Graphpad). A simple linear regression model
493 for the ADP calibration curve was used to determine the relationship between luminescence
494 and ADP concentration. Non-linear regression analysis (typically Agonist vs. response (three
495 parameters) was used in Hemin/BTdCPU experiments.
496
497 *AlphaFold Prediction:* The human HRI sequence was used as a basis for AlphaFold 3[28], with
498 2 copies being set as a parameter for dimerization. Heme was also included for prediction of
499 Heme binding sites.
500
501 *Mass Photometry:* Mass determination of solution phase HRI and phosphorylated HRI
502 Hemin was conducted using a Refeyn TwoMP instrument. Experimental data were collected
503 using Grace Bio-Labs Culture Well Reusable 50-3mm DIA x 1mm Depth Gaskets and High
504 Precision glass microscope slides, repeatedly cleaned in ultrapure water and isopropanol
505 and dried using a stream of nitrogen gas. Data were obtained through the collection of mass
506 photometry videos. Prior to HRI data collection, mass calibration was conducted using BSA
507 (66 kDa) and aldolase (160 kDa). By fitting Gaussian functions to ratiometric contrast values
508 obtained from the protein standards using the DiscoverMP v2.5 software (Refeyn), a linear
509 mass calibration was obtained. HRI proteins were diluted to the stated concentrations in 20
510 μL 20 mM HEPES pH 7.5, 150 mM NaCl, 5 mM $MgCl_2$ and 2 mM TCEP, placed on the slide,
511 and then a one-minute mass photometry video was collected. Data was analysed using the
512 DiscoveryMP v2.5 (Refeyn) software.
513
514 *Thermal Unfolding Assays:* Thermal Unfolding Assays were conducted using a NanoTemper
515 Panta using Prometheus Standard Capillaries (NanoTemper) (PR-C002). Briefly, HRI was
516 defrosted, and centrifuged at 20,000 g for 10 minutes, and then diluted to 0.2 mg/mL in 20

517 mM HEPES pH 7.5, 150 mM NaCl, 1 mM TCEP Buffer was incubated with Hemin/BTdCPU
518 on ice for 45 minutes before analysis. A gradient of 1 ºC/min was applied to the sample
519 starting from 25 ºC to 85 ºC. Fluorescence at 330 nm and 350 nm was monitored using an
520 excitation wavelength of 280 nm. Data analysis and identification of inflection points/TMs
521 was conducted using the Panta Analysis Software (NanoTemper).
522
523 *HRI Autophosphorylation Assay and Mass Spectrometry:* Lambda phosphatase treated HRI
524 was produced as detailed above. 1 mg/ mL HRI was incubated with 200 µM ATP (Promega)
525 for 1 hour at room temperature, before being quenched with SDS-PAGE Loading buffer and
526 running on a 4-12% NuPAGE BisTris Gel (Invitrogen) in MES SDS buffer for 45 minutes.
527 Bands corresponding to the gel shifted HRI protein (there was no protein at the lower, non-
528 phosphorylated starting migration) were excised from the gel and sent for mass
529 spectrometry analysis. Briefly, gel bands were washed sequentially in for 15 min at RT in ~
530 200 µL of 1:1 MPW/Acetonitrile (ACN), 100 mM Ammonium Bicarbonate (Ambic), 1:1
531 Ambic/ACN, then a final wash in ACN before desiccation in SpeedVac for 10 min. Bands
532 were then reduced in 10 mM DTT, 20 mM Ambic for 60 at 56 ºC, followed by a wash in 50
533 mM Indole-3-acetic acid, 20 mM Ambic for 30 min at RT. Bands were then washed in the
534 Ambic, Ambin/ACN, and ACN for 15 min before drying again with the speedvac. Gels were
535 then digested using Trypsin (Pierce) at 12.5 µg/mL, 20 mM Ambic, overnight at 30 ºC.
536 Peptides were then extracted via incubation with ACN for 15 min. The gel was then
537 centrigued, and peptides recovered from the supernatant. To this solution 5% formic acid
538 was added and incubated at for 45 minutes. Samples were dried down, and then
539 reconstituted with 10 µL 5% Formic Acid/ 10 % ACN, and then diluted with 40 µL of MPW.
540 Solutions were then analysed by a mass spectrometry using a Thermo QExactive Plus
541 Orbitrap. Data was processed using Mascot[46]. Only peptides with ppm scores <5, Ion
542 Scores >30, and unambiguous MS/MS assignment of phosphorylation modification
543 assignment were included in results. Experiments were conducted in triplicate, and only
544 assignments found in all three repeats are included in the results.
545
546 *HDX-MS Sample Preparation:* 5 µM HRI was incubated with or without 100 µM
547 Hemin/Dabrafenib for 30 minutes in Protein Dilution Buffer (20 mM HEPES pH 7.5, 150 mM
548 NaCl, 2 mM TCEP). 5 µL of this sample was diluted with 55 µL of Deuteration Buffer (20 mM
549 HEPES pH 7.5, 150 mM NaCl, 2 mM TCEP, 1% DMSO, 96.5 % D2O) (final D2O
550 concentration = 85.95%) for timepoints 3/ 30/ 300/ 3000 s, before being quenched with 20
551 µL of ice-cold Quench Solution (6 M Urea, 2% Formic Acid), and being snap frozen in liquid
552 nitrogen and stored at – 70 ºC. A further timepoint, 0.3 s, was achieved by incubating both
553 the sample and deuteration buffer on ice and then conducting a 3 s exchange reaction. Each
554 exchange reaction was conducted independently four times. A maximally deuterated control
555 where denatured HRI was incubated in 98% D_2O for 24 h was also conducted to correct for
556 back-exchange.
557
558 *HDX-MS Data Acquisition:* Data acquisition was conducted broadly as previously described
559 ([47]). Samples were rapidly thawed at room temperature and then injected into automated
560 HDX-MS fluidics and UPLC manager system (Waters). Samples were loaded into a 50 µL
561 loop and then subsequently digested using a Waters Enzymate BEH Pepsin Column (Part
562 No. 186007233) in a 0.1 % Formic Acid solution with a flow rate of 200 µL/min at 20 ºC.
563 Peptic peptides then flowed onto a Waters ACQUITY UPLC BEH C18 VanGuard Pre-
564 Column at 1 ºC (Part No. 186003975). After digestion, the flowpath was changed to elute
565 the peptides via a Waters ACQUITY UPLC BEH C18 1.7 µm 1.0 x 100 mm reverse phase
566 column (Part No. 186002346). A gradient from 0-85% 0.1% Formic Acid/ Acetonitrile,
567 conducted at 1 ºC with a 40 µL/min flowrate was used to elute deuterated peptides which
568 were then ionised using an ESI source. Mass spectrometry data were collected using a
569 Waters Select Series cIMS instrument, from a 50-2,000 m/z range with the instrument in
570 HDMSe mode. A single pass of the cyclic ion mobility separator (with a cycle time of 47 ms)

571 was conducted. A blank sample of protein dilution buffer with quench was run between
572 samples, and carryover was routinely checked to be <1% intensity of the prior sample.
573
574 *HDX-MS Data Analysis:* Peptide sequence identification was conducted using Protein Lynx
575 Global Server (Waters). Minimum inclusion criteria were a minimum intensity of 5000 counts,
576 minimum sequence length 5, maximum sequence length 35, a minimum of 3 fragment ions,
577 a minimum of 0.1 products per amino acid, a minimum score of 5.0, a maximum MH+ Error
578 of 10 ppm. Subsequent analysis and determination of deuteration values conducted using
579 HDExaminer (Sierra Analytics/Trajan). Experimental design, data acquisition, analysis, and
580 reporting are in line with the community agreed recommendations[48]. HDX-MS date were
581 represented on the Alphafold 3 generated structure of HRI or HRI kinase domain using
582 PyMOL Molecular Graphics System, Version 3.0 (Schrödinger).
583
584
585

Acknowledgements
GRM thanks Dr Anna Plechanovova and Prof. Ron Hay for help with Mass Photometry. GRM thanks Dr Olawale Raimi for helpful input, reading of the manuscript and help with aspects of the investigation. This work was funded by The Royal Society, research grant: RGS\R1\231147. HDX-MS equipment was funded by BBSRC Capital Equipment Fund BB/V019635/1. VV is supported by an MRC iCase Studentship (grant number MR/R01579/1). This work was supported by the Michael J. Fox Foundation (M.M.K.M). We thank the MRC PPU Reagents and Services facility (MRC I PPU, College of Life Sciences, University of Dundee, Scotland, mrcppureagents.dundee.ac.uk) for the reagents and/or services indicated in this publication. We thank Hajara Lawal of the Fingerprints proteomics services, School of Life Sciences, Dundee, for their help with phosphorylation analysis of HRI, and Douglas Lamont for his continued support of the HDX-MS facility.

CRediT Author Contribution
Shivani Kanta, Investigation **Vanesa Vinciauskaite**: Resources, Writing — review and editing **Graham Neill:** Investigation **Miratul M.K. Muqit:** Writing — review and editing. **Glenn R Masson**: Conceptualisation, Resources, Supervision, Investigation, Funding acquisition, Methodology, Writing — original draft, Project administration, Writing — review and editing.

Table 1: Autophosphorylation sites detected in human HRI.

Position	Peptide Sequence	P-Site	*m/z*	z	M_r (experimental)	M_r (calculated)	Ion Score	ID'd Prior?
-24-10**	MAHHHHHHSSGSENLYFQGSHMEFMQGGNSGVRK	S6	1344.4661		4030.3764	4030.3719	35	Yes[37]
11-52	REEEGDGAGAVAAPPAIDFPAEGPDPEYDESDVPAEIQVLKE	S41	1044.4710	4	4173.8551	4173.8467	49	Yes[37]
92-118	KLLCQTFIKMGLLSSFTCSDEFSSLRL	T97	1532.1959	2	3062.3773	3061.4000	61	Yes[37]
100-123	KMGLLSSFTCSDEFSSLRLHHNRA	S114 S115	919.0630	3	2754.1671	2753.1492	63	
134-146	RVRQDPCEDISRI	S144	727.8105	2	1453.6065	1453.6021	58	Yes[37]*
150-163	RSREVALEAQTSRY	S151	476.2280	3	1425.6623	1425.6613	51	
150-163	RSREVALEAQTSRY	T160	476.2286	3	1425.6618	1425.6613	68	Yes[37]
187-198	KLDGQYYAIKKI	Y192	639.8118	2	1277.6091	1277.6057	61	Yes[37]
187-198	KLDGQYYAIKKI	Y193	639.8109	2	1277.6073	1277.6057	52	Yes[37]
256-265	RAAIELPSLEVLSDQEEDRE	S253 S258	1087.4687	2	2172.9229	2172.9228	50	Yes[37]
256-265	RAAIELPSLEVLSDQEEDRE	S258	1047.4882	2	2092.9618	2092.9565	82	Yes[37]
270-289	KNDESSSSSIIFAEPTPEKE	S275	1009.4376	2	2016.8606	2016.8565	106	Yes[37]
270-289	KNDESSSSSIIFAEPTPEKE	S276 S277 S278	1089.4030	2	2176.7914	2176.7891	58	Yes[37]
291-307	RFGESDTENQNNKSVKY	S295 T297 S304	968.8440	2	1935.6735	1935.6690	54	Yes[37]*
303-315	KSVKYTTNLVIRE	T308 T309	485.2330	3	1452.6771	1452.6779	34	
401-422	RGREYVDESACPYVMANVATKI	Y405	1171.0101	2	2340.0057	2338.9963	66	
401-422	RGREYVDESACPYVMANVATKI	S409	780.6738	3	2338.9999	2338.9963	95	
401-421	RGREYVDESACPYVMANVATK	Y405 S409	864.6954	3	2591.0644	2591.0587	54	
401-422	RGREYVDESACPYVMANVATKI	Y413	780.6747	3	2339.0021	2338.9963	48	
458-473	KIGDFGLACTDILQKN	T467	815.8801	2	1629.7457	1629.7474	70	
458-480	KIGDFGLACTDILQKNTDWTNRN	T477	840.3826	3	2518.1261	2518.1199	71	
481-511	KRTPTHTSRVGTCLYASPEQLEGSEYDAKS	T486 T488 S489 T493	1158.4593	3	3472.3561	3472.3486	49	Yes[27]
481-511	KRTPTHTSRVGTCLYASPEQLEGSEYDAKS	S489 T493 Y496 S498	1158.7914	3	3473.3523	3473.3326	36	
490-511	RVGTCLYASPEQLEGSEYDAKS	S505	766.3301	3	2295.9686	2295.9606	40	
533-551	RAEVLTGLRTGQLPESLRK	T538 T542 S548	694.3163	3	2079.9270	2078.9204	32	Yes[37] *
558-566	KYIQHLTRR	T564	505.7444	2	1009.4743	1009.4746	31	
571-597	RPSAIQLLQSELFQNSGNVNLTLQMKI	S586	957.1422	2	2868.4046	2868.4092	82	
609-622	KQLNLLSQDKGVRD	S615	725.8770	2	1449.7394	1449.7341	56	Yes[37]

Table 1 = Autophosphorylation sites detected in human HRI. * = detected in mouse HRI.
**= Identified in peptides containing the N-terminal His-tag

615 **Table 2 HDX-MS Statistics**
616

	Apo	Dabrafenib	Hemin
# of Peptides	218	218	218
Coverage	89.3%	89.3%	87.9%
Gaps of Coverage	41-46, 66-72, 96-98, 106-113,366-389, 381-392, 516-521, 615-630		
Av. Length	14.1	14.1	14.1
Redundancy	4.7	4.7	5.1
Time Points	0.3 s*,3 s, 30 s**, 300 s**, 3000 s**		
Replicates	ND 4, Deuterated 3		
Controls	Maximally Deuterated (APO) Control		
Replicability	1.08%***	0.94%	0.97%****
Significance threshold			

617
618 *= 0.3 s timepoint created by pipetting 3 s by hand at with ice-cold solutions.
619 **= conducted by liquid handling robot
620 ***=Mean standard deviation between replicates
621 **** = for peptides exhibiting EX2 kinetics only.
622
623

624 1. Chen, J.-J. Regulation of protein synthesis by the heme-regulated eIF2α kinase: relevance to
625 anemias. *Blood* **109**, 2693–2699 (2006).

626 2. Zhang, S., Macias-Garcia, A., Velazquez, J. & Chen, J.-J. Heme-Regulated eIF2α Kinase
627 Coordinates Translational Repression of eIF2αP and mTORC1 Signaling during Iron Deficiency to
628 Mitigate Ineffective Erythropoiesis. *Blood* **128**, 1037 (2016).

629 3. Ricketts, M. D., Emptage, R. P., Blobel, G. A. & Marmorstein, R. The heme-regulated inhibitor
630 kinase requires dimerization for heme-sensing activity. *J Biol Chem* **298**, 102451 (2022).

631 4. Rafie-Kolpin, M. *et al.* Two Heme-binding Domains of Heme-regulated Eukaryotic Initiation
632 Factor-2α Kinase N TERMINUS AND KINASE INSERTION*. *J. Biol. Chem.* **275**, 5171–5178
633 (2000).

634 5. Fagard, R. & London, I. M. Relationship between phosphorylation and activity of heme-regulated
635 eukaryotic initiation factor 2 alpha kinase. *Proc. Natl. Acad. Sci.* **78**, 866–870 (1981).

636 6. Sekine, Y. *et al.* A mitochondrial iron-responsive pathway regulated by DELE1. *Mol. Cell* **83**,
637 2059-2076.e6 (2023).

638 7. Fessler, E. *et al.* A pathway coordinated by DELE1 relays mitochondrial stress to the cytosol.
639 *Nature* 1–5 (2020) doi:10.1038/s41586-020-2076-4.

640 8. Yang, J. *et al.* DELE1 oligomerization promotes integrated stress response activation. *Nat. Struct.*
641 *Mol. Biol.* **30**, 1295–1302 (2023).

642 9. Guo, X. *et al.* Mitochondrial stress is relayed to the cytosol by an OMA1–DELE1–HRI pathway.
643 *Nature* 1–6 (2020) doi:10.1038/s41586-020-2078-2.

644 10. Perea, V. *et al.* Pharmacologic activation of a compensatory integrated stress response kinase
645 promotes mitochondrial remodeling in PERK-deficient cells. *Cell Chem. Biol.* **30**, 1571-1584.e5
646 (2023).

647 11. Chakrabarty, Y., Yang, Z., Chen, H. & Chan, D. C. The HRI branch of the integrated stress
648 response selectively triggers mitophagy. *Mol. Cell* (2024) doi:10.1016/j.molcel.2024.01.016.

649 12. Singh, P. K. *et al.* Genetic screening identifies integrated stress response kinase HRI (EIF2AK1)
650 as a negative regulator of PINK1 and mitophagy signalling. *bioRxiv* 2023.03.20.533516 (2023)
651 doi:10.1101/2023.03.20.533516.

652 13. Yerlikaya, A., Kimball, S. R. & Stanley, B. A. Phosphorylation of eIF2α in response to 26S
653 proteasome inhibition is mediated by the haem-regulated inhibitor (HRI) kinase. *Biochem. J.* **412**,
654 579–588 (2008).

655 14. Inoue, Y. *et al.* Abstract 1233: Novel inhibitor targeting triple integrated stress response kinase
656 HRI, PERK, and GCN2 provides new insights into overcoming resistance to proteasome inhibitors in
657 multiple myeloma. *Cancer Res.* **84**, 1233–1233 (2024).

658 15. Mukherjee, T. *et al.* The eIF2α kinase HRI triggers the autophagic clearance of cytosolic protein
659 aggregates. *J. Biol. Chem.* **296**, 100050 (2021).

660 16. Burwick, N. & Aktas, B. H. The eIF2-alpha kinase HRI: a potential target beyond the red blood
661 cell. *Expert Opin Ther Tar* **21**, 1171–1177 (2017).

662 17. Smith, K. H. *et al.* The Heme-Regulated Inhibitor Pathway Modulates Susceptibility of Poor
663 Prognosis B-Lineage Acute Leukemia to BH3-Mimetics. *Mol. Cancer Res.* **19**, 636–650 (2021).

664 18. Lough, L. *et al.* Triazolo[4,5-d]pyrimidines as Validated General Control Nonderepressible 2
665 (GCN2) Protein Kinase Inhibitors Reduce Growth of Leukemia Cells. *Comput Struct Biotechnology J*
666 **16**, 350–360 (2018).

667 19. Sannino, S. *et al.* Unique integrated stress response sensors regulate cancer cell susceptibility
668 when Hsp70 activity is compromised. *Elife* **10**, e64977 (2021).

669 20. Chen, T. *et al.* Chemical genetics identify eIF2α kinase heme-regulated inhibitor as an anticancer
670 target. *Nat Chem Biol* **7**, 610–616 (2011).

671 21. Yefidoff-Freedman, R. *et al.* Development of 1-((1,4-trans)-4-Aryloxycyclohexyl)-3-arylurea
672 Activators of Heme-Regulated Inhibitor as Selective Activators of the Eukaryotic Initiation Factor 2
673 Alpha (eIF2α) Phosphorylation Arm of the Integrated Endoplasmic Reticulum Stress Response. *J.*
674 *Med. Chem.* **60**, 5392–5406 (2017).

675 22. Denoyelle, S. *et al.* In vitro inhibition of translation initiation by N,N′-diarylureas—potential anti-
676 cancer agents. *Bioorg. Med. Chem. Lett.* **22**, 402–409 (2012).

677 23. Zhang, Q. *et al.* New activators of eIF2α Kinase Heme-Regulated Inhibitor (HRI) with improved
678 biophysical properties. *Eur J Med Chem* **187**, 111973 (2020).

679 24. Yerlikaya, A. Heme-regulated inhibitor: an overlooked eIF2α kinase in cancer investigations. *Med*
680 *Oncol* **39**, 73 (2022).

681 25. Rosen, M. D. *et al.* Discovery of the first known small-molecule inhibitors of heme-regulated
682 eukaryotic initiation factor 2α (HRI) kinase. *Bioorg. Med. Chem. Lett.* **19**, 6548–6551 (2009).

683 26. Carlson, KennethR., Georgiadis, MillieM., Tameire, F., Staschke, KirkA. & Wek, RonaldC.
684 Activation of Gcn2 by small molecules designed to be inhibitors. *J Biol Chem* 104595 (2023)
685 doi:10.1016/j.jbc.2023.104595.

686 27. Rafie-Kolpin, M., Han, A.-P. & Chen, J.-J. Autophosphorylation of Threonine 485 in the
687 Activation Loop Is Essential for Attaining eIF2α Kinase Activity of HRI †. *Biochemistry* **42**, 6536–
688 6544 (2003).

689 28. Abramson, J. *et al.* Accurate structure prediction of biomolecular interactions with AlphaFold 3.
690 *Nature* 1–3 (2024) doi:10.1038/s41586-024-07487-w.

691 29. Bauer, B. N., Rafie-Kolpin, M., Lu, L., Han, A. & Chen, J.-J. Multiple Autophosphorylation Is
692 Essential for the Formation of the Active and Stable Homodimer of Heme-Regulated eIF2α Kinase †.
693 *Biochemistry* **40**, 11543–11551 (2001).

694 30. Ciudad, M. T. *et al.* Dabrafenib alters MDSC differentiation and function by activation of GCN2.
695 *Cancer Res. Commun.* **4**, 765–784 (2024).

696 31. Nagasawa, I., Kunimasa, K., Tsukahara, S. & Tomida, A. BRAF-mutated cells activate GCN2-
697 mediated integrated stress response as a cytoprotective mechanism in response to vemurafenib.
698 *Biochem. Biophys. Res. Commun.* **482**, 1491–1497 (2017).

699 32. Fujimoto, J. *et al.* Identification of Novel, Potent, and Orally Available GCN2 Inhibitors with
700 Type I Half Binding Mode. *Acs Med Chem Lett* **10**, 1498–1503 (2019).

701 33. Burwick, N. *et al.* The eIF2-alpha kinase HRI is a novel therapeutic target in multiple myeloma.
702 *Leuk. Res.* **55**, 23–32 (2017).

703 34. Waizenegger, I. C. *et al.* A Novel RAF Kinase Inhibitor with DFG-Out–Binding Mode: High
704 Efficacy in BRAF-Mutant Tumor Xenograft Models in the Absence of Normal Tissue
705 Hyperproliferation. *Mol. Cancer Ther.* **15**, 354–365 (2016).

706 35. Igarashi, J. *et al.* Elucidation of the Heme Binding Site of Heme-regulated Eukaryotic Initiation
707 Factor 2α Kinase and the Role of the Regulatory Motif in Heme Sensing by Spectroscopic and
708 Catalytic Studies of Mutant Proteins*. *J. Biol. Chem.* **283**, 18782–18791 (2008).

709 36. Saraste, M., Sibbald, P. R. & Wittinghofer, A. The P-loop — a common motif in ATP- and GTP-
710 binding proteins. *Trends Biochem. Sci.* **15**, 430–434 (1990).

711 37. Igarashi, J. *et al.* Autophosphorylation of heme-regulated eukaryotic initiation factor 2α kinase
712 and the role of the modification in catalysis. *FEBS J.* **278**, 918–928 (2011).

713 38. Walte, A. *et al.* Mechanism of dual specificity kinase activity of DYRK1A. *FEBS J.* **280**, 4495–
714 4511 (2013).

715 39. Nolen, B., Taylor, S. & Ghosh, G. Regulation of Protein Kinases Controlling Activity through
716 Activation Segment Conformation. *Mol. Cell* **15**, 661–675 (2004).

717 40. Aranda, S., Laguna, A. & Luna, S. de la. DYRK family of protein kinases: evolutionary
718 relationships, biochemical properties, and functional roles. *FASEB J.* **25**, 449–462 (2011).

719 41. Gizzio, J., Thakur, A., Haldane, A., Post, C. B. & Levy, R. M. Evolutionary sequence and
720 structural basis for the distinct conformational landscapes of Tyr and Ser/Thr kinases. *Nat. Commun.*
721 **15**, 6545 (2024).

722 42. Poulikakos, P. I., Zhang, C., Bollag, G., Shokat, K. M. & Rosen, N. RAF inhibitors transactivate
723 RAF dimers and ERK signalling in cells with wild-type BRAF. *Nature* **464**, 427–430 (2010).

724 43. Bhavnani, V. *et al.* Elucidation of molecular mechanism of stability of the heme-regulated eIF2α
725 kinase upon binding of its ligand, hemin in its catalytic kinase domain. *J. Biomol. Struct. Dyn.* **36**,
726 2845–2861 (2018).

727 44. Szaruga, M. *et al.* Activation of the integrated stress response by inhibitors of its kinases. *Nat.*
728 *Commun.* **14**, 5535 (2023).

729 45. Inglis, A. J. *et al.* Activation of GCN2 by the ribosomal P-stalk. *Proc National Acad Sci* **116**,
730 201813352 (2019).

731 46. Perkins, D. N., Pappin, D. J., Creasy, D. M. & Cottrell, J. S. Probability-based protein
732 identification by searching sequence databases using mass spectrometry data. *Electrophoresis* **20**,
733 3551–67 (1999).

734 47. Gong, G. Q. *et al.* A small-molecule PI3Kα activator for cardioprotection and neuroregeneration.
735 *Nature* 1–10 (2023) doi:10.1038/s41586-023-05972-2.

736 48. Masson, G. R. *et al.* Recommendations for performing, interpreting and reporting hydrogen
737 deuterium exchange mass spectrometry (HDX-MS) experiments. *Nature methods* **16**, 595–602
738 (2019).

739

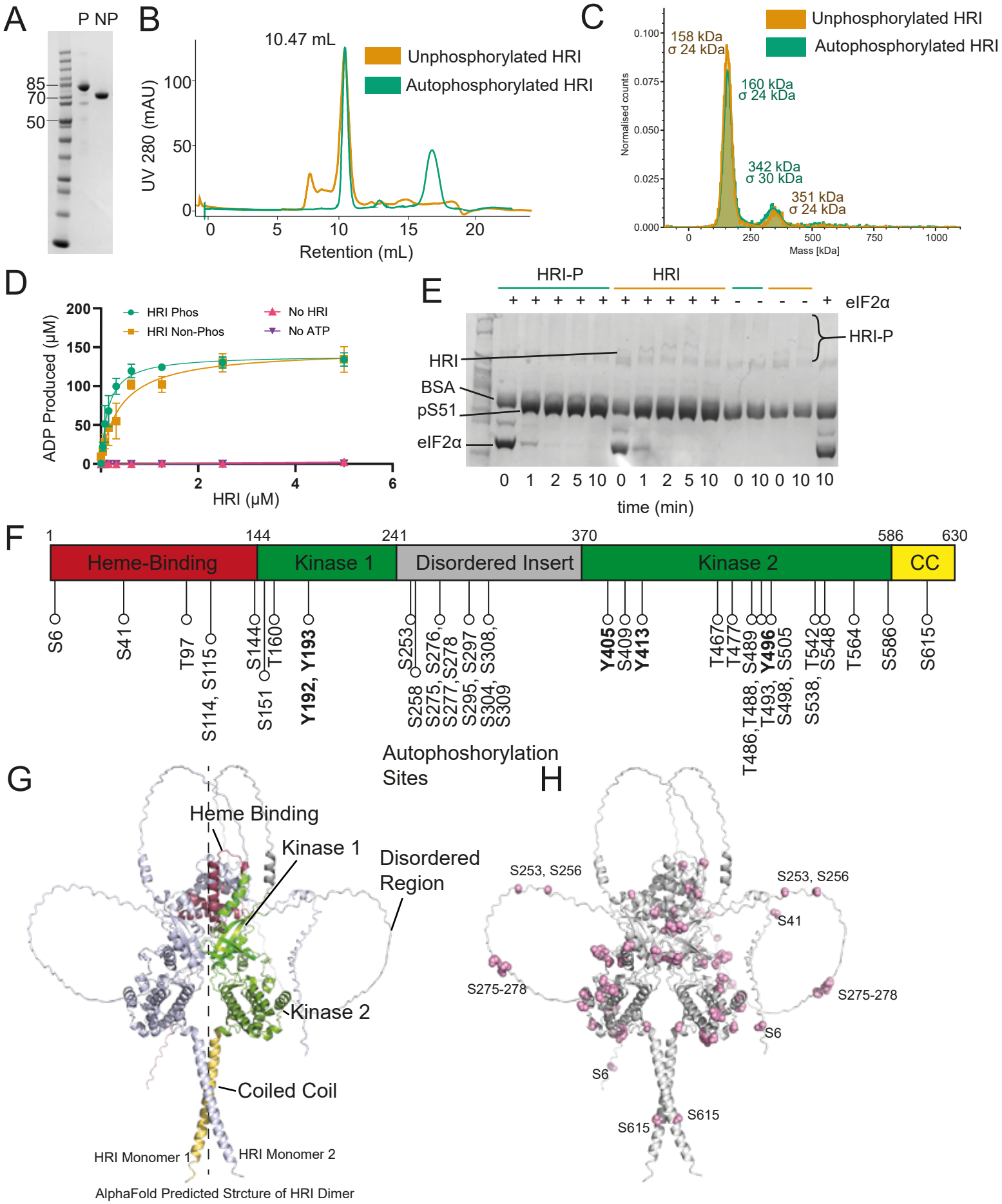

Figure 1: Characterisation of the phosphorylated HRI dimer (A): Purified recombinant HRI run on an SDS-PAGE gel in both phosphorylated (P) and lambda protein phosphate dephosphorylated (NP) protein (B) Size-Exclusion Chromatography of Phosphorylated and dephosphorylated HRI both of which elute with a retention volume of 10.47 mL (C) Mass Photometry analysis of HRI. Both P and NP HRI have a predominant population of ~150 kDa, indicative of a dimeric oligomerisation state. (D) ADP-GLO Kinase assay of HRI P and NP. (E) Phos-Tag Gel of HRI assay. Both phosphorylation of substrate (recombinant human eIF2α) and autophosphorylation can be seen. (F) Sites of HRI autophosphorylation. (G) AlphaFold 3 model of Apo HRI dimer, with domains highlighted. The dashed line shows the approximate line of 2-fold symmetry. (H) Locations of autophosphorylated residues on HRI, with those on the periphery of highlighted.

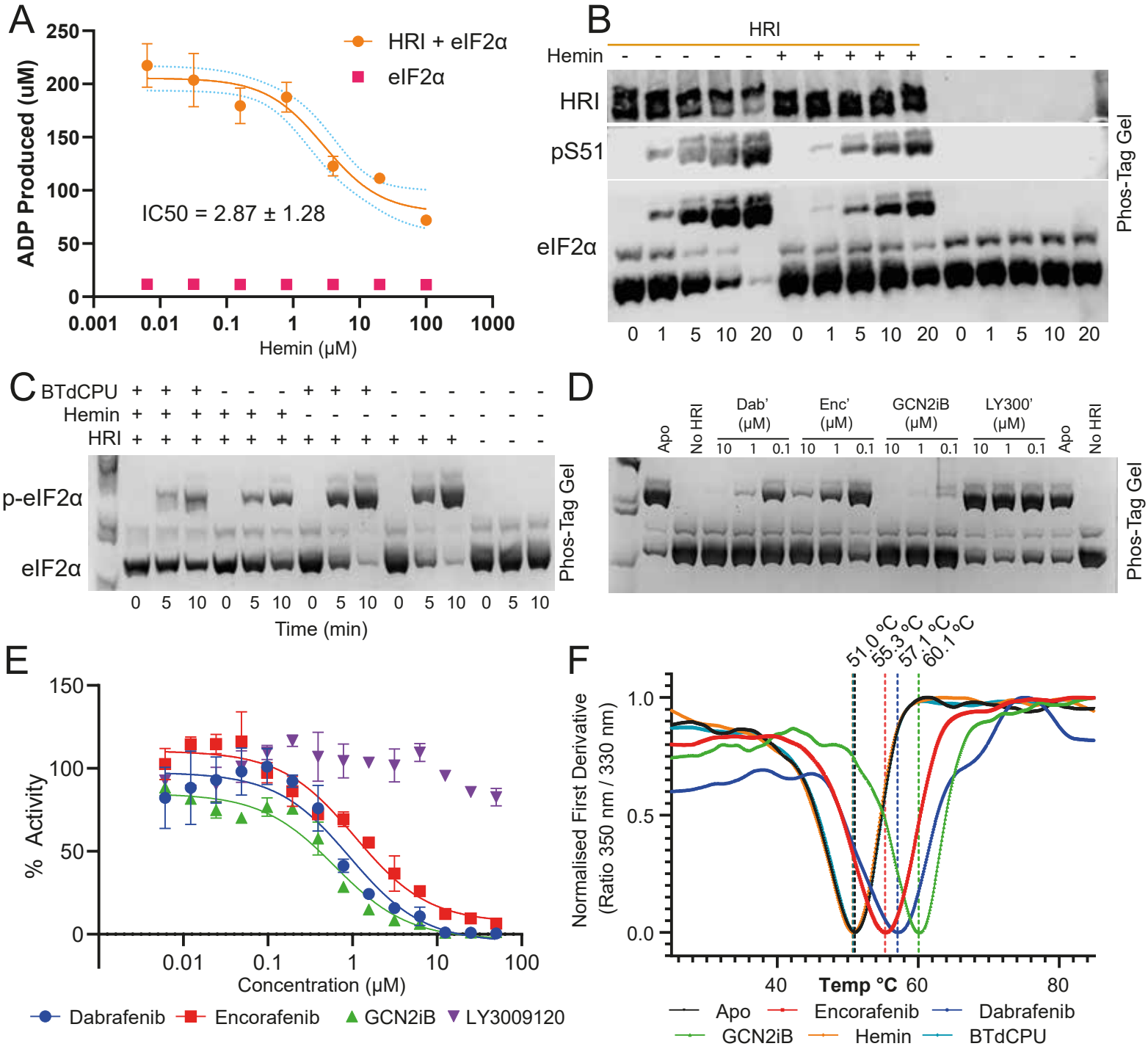

Figure 2: Characterisation of HRI modulators (A) ADP-GLO kinase assay with a concentration gradient of Hemin using recombinant eIF2α as a substrate– an IC50 of 2.87 ± 1.28 μM was determine. No activity was detected in the absence of HRI (eIF2α only control). (B) Western-Blot assay from a Phos-Tag separated HRI kinase assay using eIF2α substrate to observe Hemin effects on both autophosphorylation and substate phosphorylation. The total eIF2α probe shows the development of phosphorylated eIF2α over the course of the reaction, reduced in the presence of Hemin. The S51 phosphorylation specific antibody probe shows the gradual production of phosphorylated substrate from HRI. HRI moves to a higher band (indicative of phosphorylation) upon addition of ATP – this is inhibited upon addition of Hemin. (C) Phos-tag analysis of the effects of Hemin and BTdCPU on eIF2α phosphorylation. (D) Phos-tag analysis of RAFi and GCN2iB. (E) ADP-GLO analysis of HRI activity against RAFi and GCN2iB. (F) nanoDSF analysis of 5 μM Hemin, 10 μM BTdCPU, 10 μM Dabrafenib, 10 μM Encorafenib and 10 μM GCN2iB. TMs (as determined as the nadir of the first derivative of the ratio of the 350/ 330 nm curve) are shown above

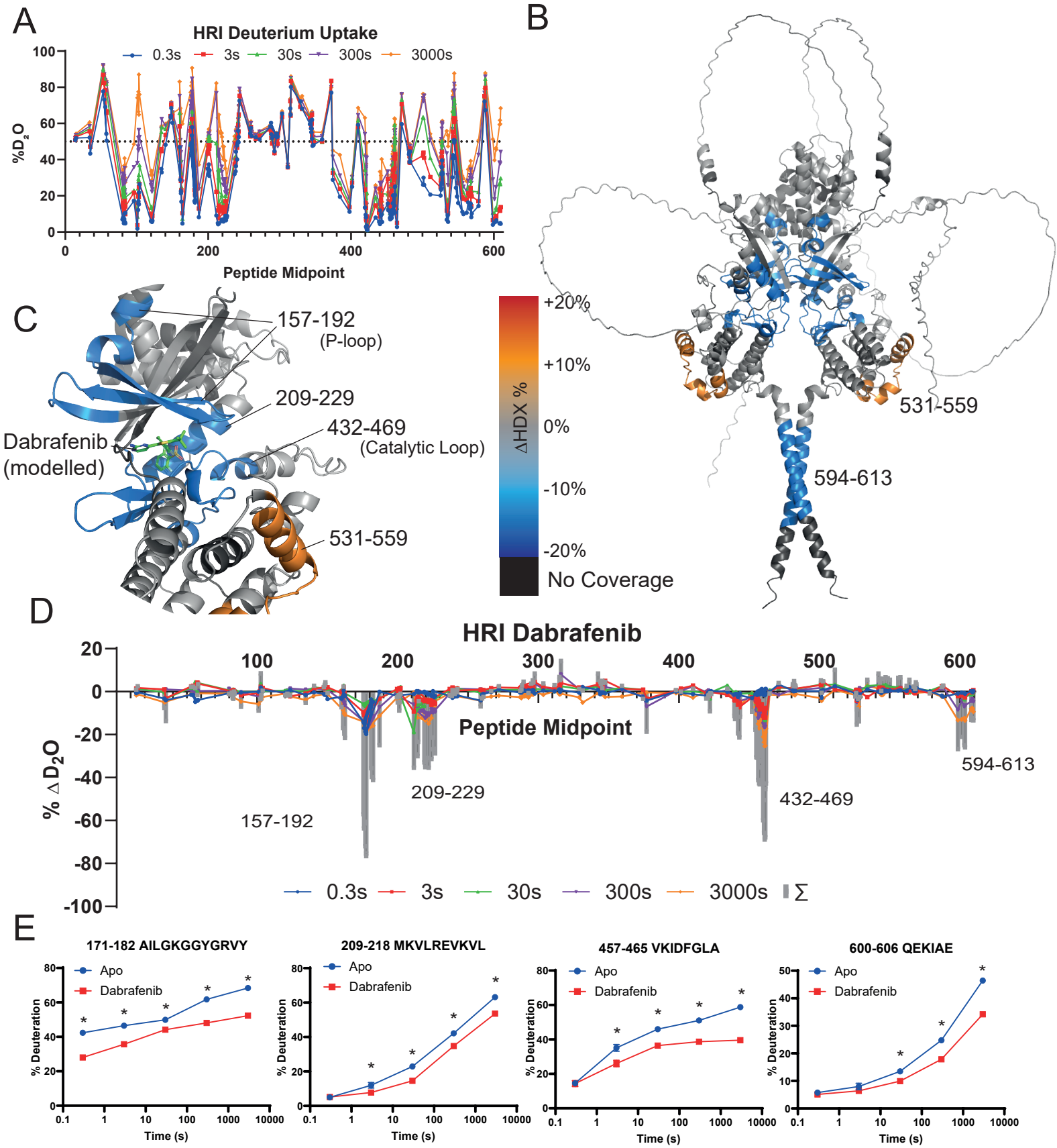

Figure 3: HDX-MS analysis of Dabrafenib Binding (A) Global Exchange profile of Apo Dimeric dephosphorylated HRI over five timepoints. The dashed line at 50% - typically peptides with >50% exchange at the 0.3s timepoint (blue points) are disordered regions (B) HRI kinase domain with Dabrafenib binding modelled. Peptides which exhibited a reduction of solvent exchange upon Dabrafenib binding are highlighted in blue. (C) Inset of the kinase domain of HRI, showing solvent exchange changes upon Dabrafenib binding. Dabrafenib docked using a BRAF model (PDB:5CSW) (D) HDX-MS plot of Dabrafenib binding to HRI. Summed difference over all five timepoints (E) Selected peptides exhibiting differences in solvent uptake upon Dabrafenib binding. * = > 5%/0.5Da difference and passes a student t-test with p = 0.05 (or lower).

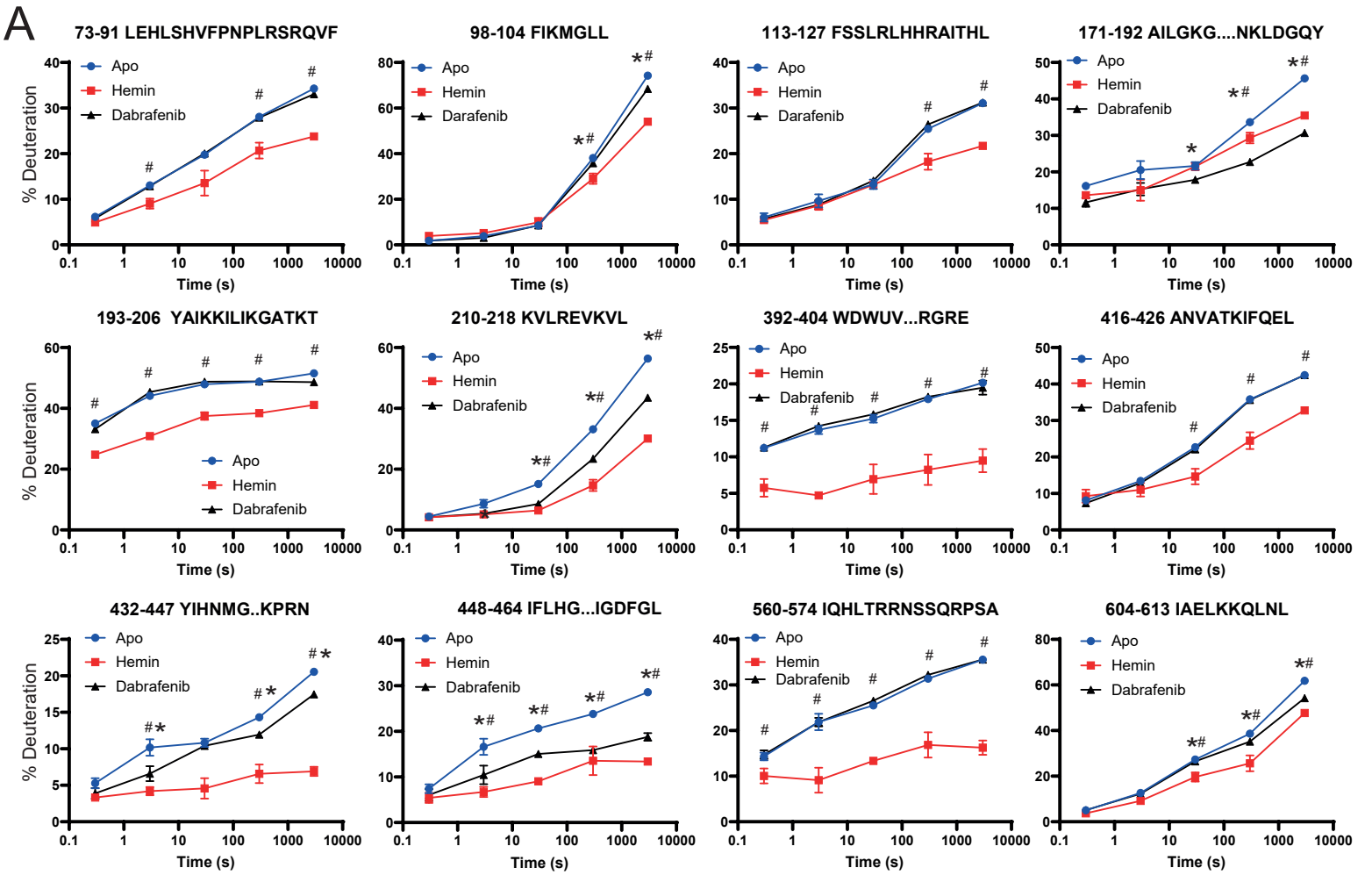
A
73-91 LEHLSHVFPNPLRSRQVF
98-104 FIKMGLL
113-127 FSSLRLHHRAITHL
171-192 AILGKG....NKLDGQY
193-206 YAIKKILIKGATKT
210-218 KVLREVKVL
392-404 WDWUV...RGRE
416-426 ANVATKIFQEL
432-447 YIHNMG..KPRN
448-464 IFLHG...IGDFGL
560-574 IQHLTRRNSSQRPSA
604-613 IAELKKQLNL
Apo
Hemin
Dabrafenib
Darafenib
% Deuteration
Time (s)

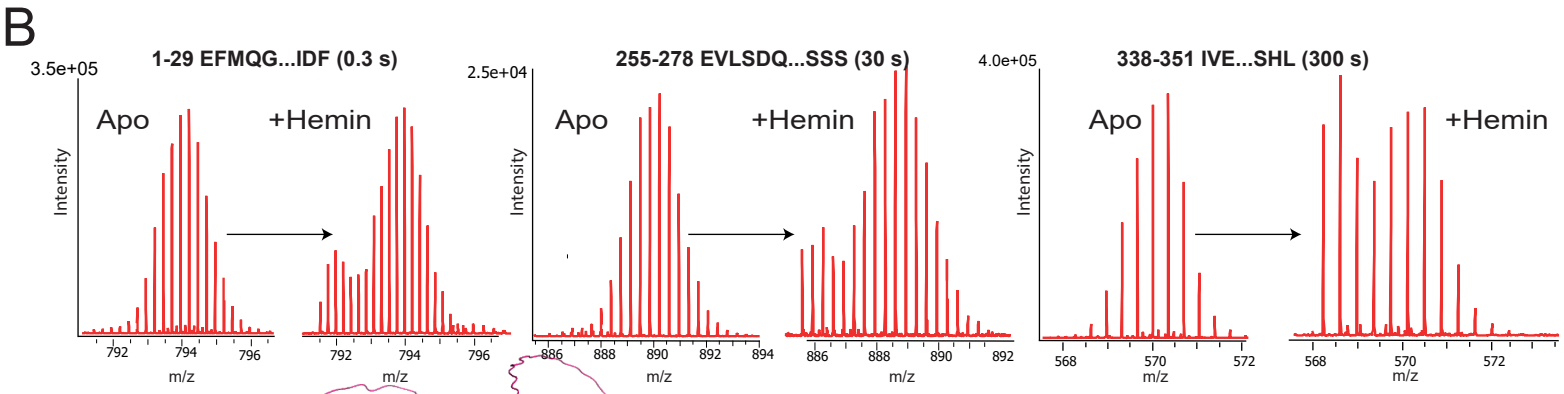
B
1-29 EFMQG...IDF (0.3 s)
255-278 EVLSDQ...SSS (30 s)
338-351 IVE...SHL (300 s)
Apo
+Hemin
Intensity
m/z

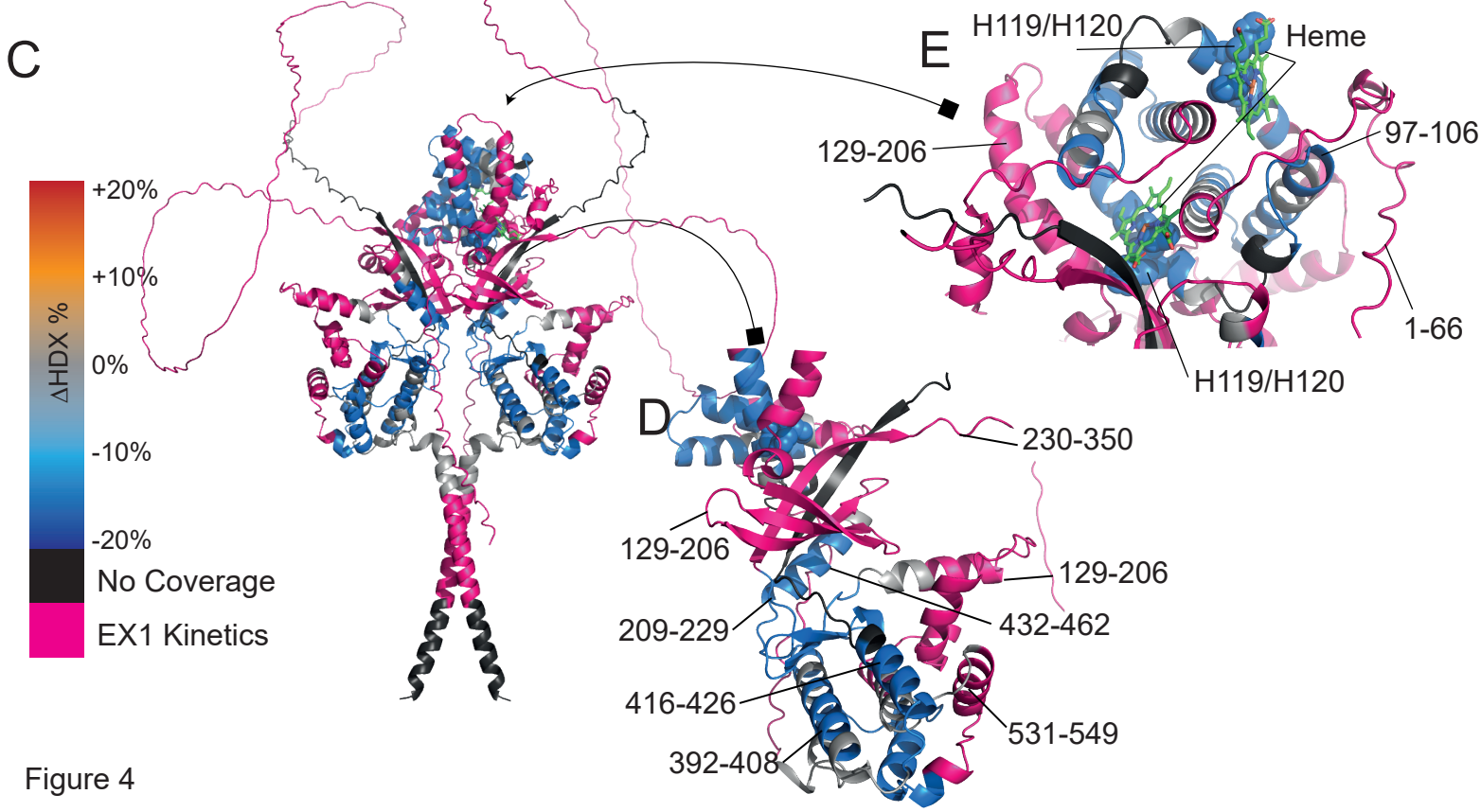
C
D
E
+20%
+10%
0%
-10%
-20%
ΔHDX %
No Coverage
EX1 Kinetics
H119/H120
Heme
129-206
97-106
1-66
230-350
209-229
432-462
416-426
531-549
392-408

Figure 4

Figure 4: HDX-MS analysis of Hemin Binding (A) A selection of peptides detailing the solvent uptake differences upon Hemin and Dabrafenib binding. * = > 5%/0.5Da difference and passes a student t-test with p = 0.05 (or lower) with Dabrafenib binding when compared to Apo HRI. # = > 5%/0.5Da difference and passes a student t-test with p = 0.05 (or lower) with Hemin binding when compared to Apo HRI. (B) Spectra of selected peptides exhibiting EX1 kinetics which emerge on Hemin binding. (C) HDX-MS data mapped onto an AlphaFold Model with Heme docking. Representations of EX1 kinetics in three peptides found within the regions indicated as pink. (D) Kinase domain upon Hemin binding. (E) HDX-MS data around the Heme Binding Domain. Two previously identified residues, Histidine 119 and 120, are highlighted and represented as spheres.

```
sp|P19525|E2AK2_HUMAN      GLRNNQRKAKRSLAPRFDLPDMKETKYTVDKRFGMDFKEIELIGSGGFGQVFKAKHRIDG   290 PKR
sp|Q9NZJ5|E2AK3_HUMAN      --TENKYDSVSGEANDSSWNDIKNSG--YISRYLTDFEPIQCLGRGGFGVVFEAKNKVDD   616 PERK
sp|Q9P2K8|E2AK4_HUMAN      RL---------------PSAAFFSETQRQFSRYFIEFEELQLLGKGAFGAVIKVQNKLDG   613 GCN2
sp|Q9BQI3|E2AK1_HUMAN      KI---------------RSR--EVALEAQTSRYLNEFEELAILGKGGYGRVYKVRNKLDG   190 HRI
                                                        .*:  :*: :  :* *.:* * :.::::*.

sp|P19525|E2AK2_HUMAN      KTYVIKRVKYNN------EKAEREVKALAKLDHVNIVHYNGCWDGFDYDP----------   334 PKR
sp|Q9NZJ5|E2AK3_HUMAN      CNYAIKRIRLPNRELA-REKVMREVKALAKLEHPGIVRYFNAWLEAPPEKWQEKMDEIWL   675 PERK
sp|Q9P2K8|E2AK4_HUMAN      CCYAVKRIPINPASRQ-FRRIKGEVTLLSRLHHENIVRYYNAWIERHERPAGPGT-----   667 GCN2
sp|Q9BQI3|E2AK1_HUMAN      QYYAIKRILIKGATKTVCMKVLREVKVLAGLQHPNIVGYHTAWIEHVHVIQPRADR----   246 HRI
                             *.:*::           :   **. *: *.* .** *  .*

sp|P19525|E2AK2_HUMAN      -------------------------------ETSDD------------------------   339 PKR
sp|Q9NZJ5|E2AK3_HUMAN      KDESTDWPLSSPSPMDAPS----VKIRRMDPFATKEHIEIIAPSPQRSRSFSVGISCDQT   731 PERK
sp|Q9P2K8|E2AK4_HUMAN      -------PPPDSGPLA--KDDRAARGQPASDTDGLDSVEAAAPPPILSSSVEWS-TSGER   717 GCN2
sp|Q9BQI3|E2AK1_HUMAN      ----AAIELPSLEVLSDQEEDREQCGVKNDE-SSSSSIIFAEPTPEKEKRFGESDTENQN   301 HRI
                                                          .

sp|P19525|E2AK2_HUMAN      ---------------------------------------------SL---------------   341 PKR
sp|Q9NZJ5|E2AK3_HUMAN      SSSESQFSPLEFSGMDHEDISESVDAAYNLQDSCLTDCDVEDGTMDGNDEGHSFELCPSE   791 PERK
sp|Q9P2K8|E2AK4_HUMAN      SASARFPA---------------------------TGPGSSDDE-DDDEDEHGGVF----   745 GCN2
sp|Q9BQI3|E2AK1_HUMAN      NKSVKYTTNLVI-----------------------RESGELESTLELQENGLAGLS----   334 HRI


sp|P19525|E2AK2_HUMAN      -----------------ES---------------------------SDYDPENS------   351 PKR
sp|Q9NZJ5|E2AK3_HUMAN      ASPYVRSRERTSSSIVFEDSGCDNASSKEEPKTNRLHIGNHCANKLTAFKPTSSKSSSEA   851 PERK
sp|Q9P2K8|E2AK4_HUMAN      SQSFLPAS-DSESDIIFDNEDENSK---------SQNQDEDCNEKNGCHE----------   785 GCN2
sp|Q9BQI3|E2AK1_HUMAN      ASSIV------EQQLPLRRNSHLEE---------SFTSTEESSEENVNFL----------   369 HRI
                                                                          .

sp|P19525|E2AK2_HUMAN      ----------------------KNSSRSKTKCLFIQMEFCDKGTLEQWIEKRRG------   383 PKR
sp|Q9NZJ5|E2AK3_HUMAN      TLSISPPRPTTLSLDLTKNTTEKLQPSSPKVYLYIQMQLCRKENLKDWMNGRCT------   905 PERK
sp|Q9P2K8|E2AK4_HUMAN      --------------------SEPSVTTEAVHYLYIQMEYCEKSTLRDTIDQ---------   816 GCN2
sp|Q9BQI3|E2AK1_HUMAN      ----------------------GQTEAQYHLMLHIQMQLCELSLWDWIVERNKRGREYVD   407 HRI
                                                .    *.***: *        ::

sp|P19525|E2AK2_HUMAN      ----EKLDKVLALELFEQITKGVDYIHSKKLIHRDLKPSNIFLVD-TKQVKIGDFGLVTS   438  PKR
sp|Q9NZJ5|E2AK3_HUMAN      ---IEERERSVCLHIFLQIAEAVEFLHSKGLMHRDLKPSNIFFTM-DDVVKVGDFGLVTA   961  PERK
sp|Q9P2K8|E2AK4_HUMAN      ---GLYRDTVRLWRLFREILDGLAYIHEKGMIHRDLKPVNIFLDS-DDHVKIGDFGLATD   872  GCN2
sp|Q9BQI3|E2AK1_HUMAN      ESACPYVMANVATKIFQELVEGVFYIHNMGIVHRDLKPRNIFLHGPDQQVKIGDFGLACT   467  HRI
                                     .:* :: ..: ::*.  ::****** ***:    . **:*****.

sp|P19525|E2AK2_HUMAN      LKND------GK-------------RTRSKGTLRYMSPEQIS--SQDYGKEVDLYALGLI   477  PKR
sp|Q9NZJ5|E2AK3_HUMAN      MDQD------EEEQTVLTPMPAYARHTGQVGTKLYMSPEQIH--GNSYSHKVDIFSLGLI   1013 PERK
sp|Q9P2K8|E2AK4_HUMAN      HLAFSADSKQDDQTGDLIKSDPSGHLTGMVGTALYVSPEVQGSTKSAYNQKVDLFSLGII   932  GCN2
sp|Q9BQI3|E2AK1_HUMAN      DILQKNTDWT-NRNG-----KRTPTHTSRVGTCLYASPEQLE--GSEYDAKSDMYSLGVV   519  HRI
                                   .              *   **  * ***      . *. : *:::**::

sp|P19525|E2AK2_HUMAN      LAEL-LHVCDTAFETSKFFTDLRDGII---SDIFDKK----EKTLLQKLLSKKPEDRPNT   529  PKR
sp|Q9NZJ5|E2AK3_HUMAN      LFEL-LYPFSTQMERVRTLTDVRNLKF---PPLFTQKY-PCEYVMVQDMLSPSPMERPEA   1068 PERK
sp|Q9P2K8|E2AK4_HUMAN      FFEMSYHPMVTASERIFVLNQLRDPTSPKFPEDFDDGEHAKQKSVISWLLNHDPAKRPTA   992  GCN2
sp|Q9BQI3|E2AK1_HUMAN      LLEL-FQPFGTEMERAEVLTGLRTGQL---PESLRKRC-PVQAKYIQHLTRRNSSQRPSA   574  HRI
                           : *:      *  *    :. :*          : .     :   :. :   .  .** :

sp|P19525|E2AK2_HUMAN      SEILRTLTVWKK-SPEKN----------------ER----------HTC-----------   551  PKR
sp|Q9NZJ5|E2AK3_HUMAN      INIIENAVFEDLDFPGKTVLRQRSRSLSSSGTKHSRQS-----NNSHSPL----------   1113 PERK
sp|Q9P2K8|E2AK4_HUMAN      TELLKSELLPPPQMEESELHEVLHHTLTNVDGKAYRTMMAQIFSQRISPAIDYTYDSDIL   1052 GCN2
sp|Q9BQI3|E2AK1_HUMAN      IQLLQSELFQNSGNVNLTLQMK-------------------IIEQEKE-IAELKKQLNLL   614  HRI
                            ::::..  .

                           . = Weak Conservation (< 0.5 Gonnet PAM 250 matrix)
                           : = Strong Conservation ( > 0.5 Gonnet PAM 250 matrix)
                           * = Fully Conserved
```

Supplementary Figure 1: Alignment of the kinase domains of all the human eIF2alpha kinases (PKR, PERK, HRI and GCN2).

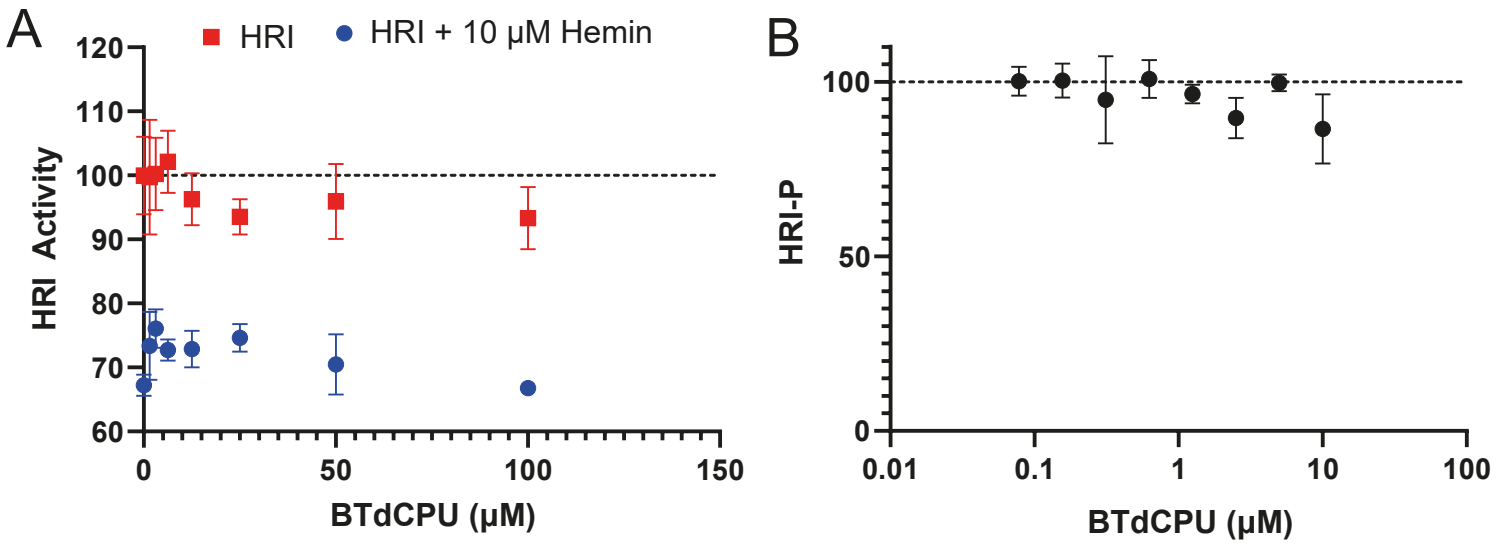

Supplementary Figure 2: BTdCPU kinase assays. (A) Activity of HRI (as measured by ADP production) on the addition of increasing BTdCPU in either the absence or presence of Hemin. (B) Autophosphorylated HRI (i.e. HRI pre-incubated with ATP and subsequently purified) was exposed to increasing BTdCPU in the presence of eIF2α. ADP levels were measured using ADP-GLO and plotted as a % of APO HRI-P levels.

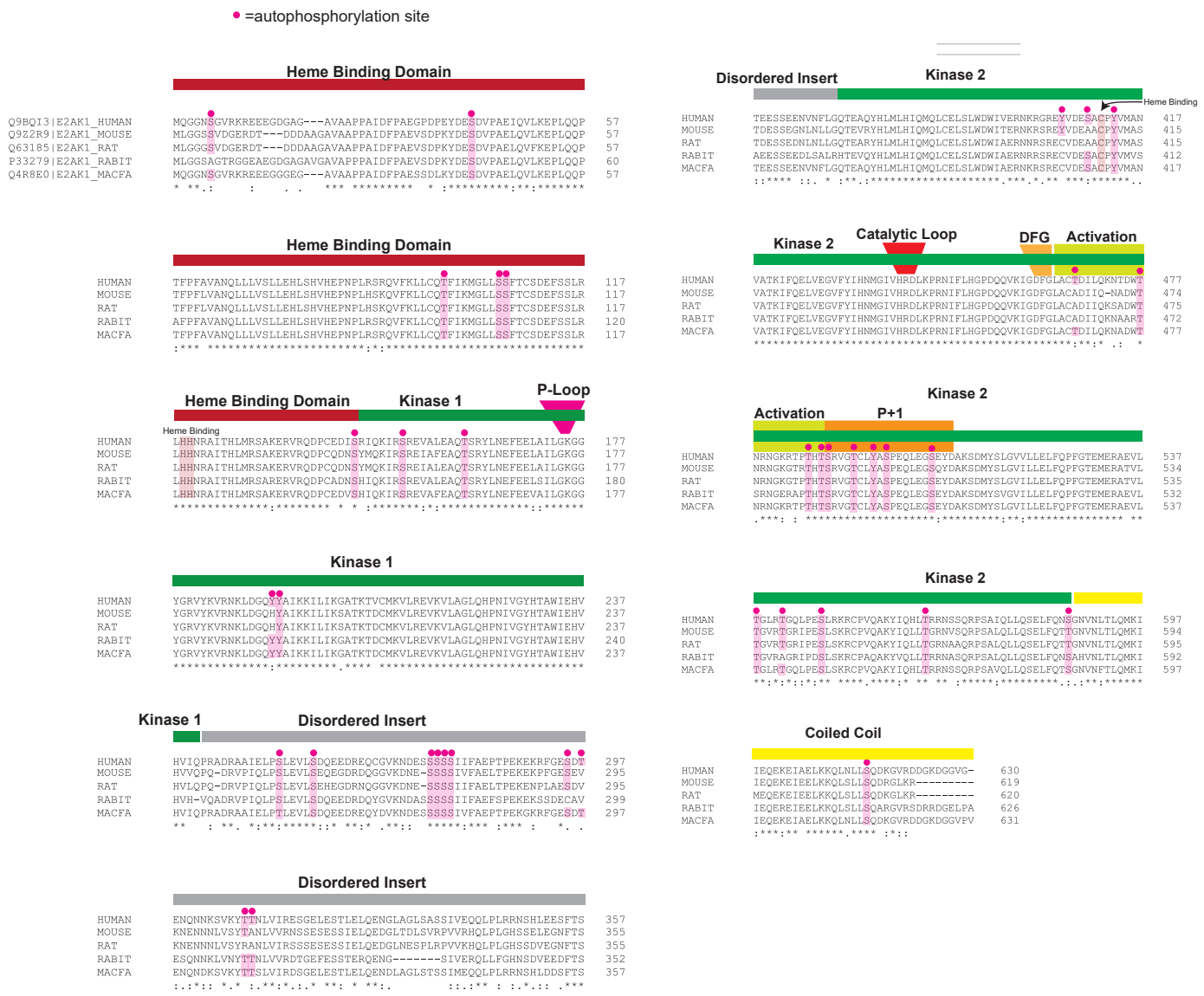

Supplementary Figure 3: Species alignment of HRI. Human (H. sapiens), Mouse (M. musculus), Rat (R. ratus), Rabbit (RABIT) and Macaca fascicularis (Crab-eating macaque) (Cynomolgus monkey) of EIF2AK1 (HRI).